

**ISOLATION AND CHARACTERIZATION  
TEMPO OXIDIZED NANOCRYSTALLINE  
CELLULOSE FROM OIL PALM EMPTY FRUIT  
BUNCH**

**ROHAIZU ROSLAN**

**UNIVERSITI SAINS MALAYSIA**

**2015**

**ISOLATION AND CHARACTERIZATION  
TEMPO OXIDIZED NANOCRYSTALLINE  
CELLULOSE FROM OIL PALM EMPTY FRUIT  
BUNCH**

**by**

**ROHAIZU ROSLAN**

**Thesis submitted in fulfillment of the requirements  
for the degree of  
Doctoral of Philosophy**

**September 2015**

## **ACKNOWLEDGEMENT**

Alhamdulillah, I am grateful and thankful to Allah S.W.T, The Great Almighty for giving me strength and guidance to complete my PhD study. Here, I would like to express my greatest gratitude to my supervisor, Professor Wan Rosli Wan Daud, for his guidance, commitment, and knowledge sharing throughout this research project.

I would like to acknowledge Universiti Sains Malaysia for the Research University grant scheme of 1001/PTEKIND/814122 and 1001/PTEKIND/845027, and Minister of Higher Education Malaysia for sponsoring my postgraduate studies. My appreciation also to all staff members of Universiti Sains Malaysia and particularly to staff of School of Industrial Technology for their helpful contribution and provides assistance directly or indirectly for this project.

I would also like to express my love to my parents and family members for their continuous support and encouragement. A special dedication also goes to all my colleagues and friends who had shared the moment together during my study period, their encouragement and moral support is precious.

## TABLE OF CONTENTS

	<b>Page</b>
<b>ACKNOWLEDGEMENT</b>	ii
<b>TABLE OF CONTENTS</b>	iii
<b>LIST OF FIGURES</b>	x
<b>LIST OF TABLES</b>	xv
<b>LIST OF ABBREVIATIONS</b>	xvi
<b>LIST OF SYMBOLS</b>	xviii
<b>LIST OF PUBLICATIONS</b>	xix
<b>ABSTRAK</b>	xx
<b>ABSTRACT</b>	xxiii
<b>CHAPTER 1: INTRODUCTION</b>	1
1.1    Project Background	1
1.2    Problem Statement	1
1.3    Objectives	3
<b>CHAPTER 2: LITERATURE REVIEW</b>	5
2.1    The Oil Palm	5
2.1.1    Oil Palm Biomass as an Alternative Source of Fiber	7
2.2    Cellulose	9
2.2.1    Molecular Structure	10
2.2.2    Supramolecular Structure	11
2.2.3    Morphological Structure	14

2.3	Nanocrystalline Cellulose (NCC)	16
2.4	Production of Nanocrystalline Cellulose	17
2.4.1	TEMPO-Mediated Oxidation	19
2.4.2	Factors that Influence the Oxidation Reaction	22
2.5	Ultrasonic Treatment	27
2.6	Potential Applications of Nanocrystalline Cellulose	29
2.6.1	Iridescent Properties of NCC Films	32
2.6.1.1	Iridescent Color Formation	34
2.6.2	Market Outlook for Nanocrystalline Cellulose	39
<b>CHAPTER 3: MATERIALS AND METHODS</b>		44
3.1	Preparation of OPEFB Dissolving Pulp	48
3.1.1	Oil Palm Empty Fruit Bunch	48
3.1.2	Pre-Hydrolysis	48
3.1.3	Soda Pulping	49
3.1.4	Total Chlorine Free Bleaching Process	49
3.1.4.1	Oxygen Bleaching	50
3.1.4.2	Ozone Bleaching	50
3.1.4.3	Peroxide Bleaching	51
3.1.5	Production of OPEFB Microcrystalline Cellulose	51
3.2	TEMPO-Mediated Oxidation	52
3.2.1	Post-Oxidation with NaClO <sub>2</sub>	52
3.3	Isolation of OPEFB Nanocrystalline Cellulose	53
3.3.1	Preparation of Different Axial Ratio of OPEFB-NCC	53

3.4	Preparation of OPEFB-NCC Film	54
3.4.1	Preparation of Different Thickness of OPEFB-NCC Film	55
3.4.2	Preparation of Plasticized OPEFB-NCC Film	55
3.4.3	OPEFB-NCC as Template	56
3.5	Characterizations Method	56
3.5.1	Determination of Carboxyl Content	56
3.5.2	Total Yield of TEMPO Oxidized OPEFB Pulp	57
3.5.3	Total Yield of OPEFB-NCC	57
3.5.4	Fourier Transform Infrared Spectroscopy	58
3.5.5	Nuclear Magnetic Resonance	58
3.5.6	X-Ray Diffraction Analysis	59
3.5.7	Transmission Electron Microscope	60
3.5.8	Scanning Electron Microscope with Energy Dispersive X-Ray	60
3.5.9	Water Retention Value	61
3.5.10	Thermogravimetric Analysis	61
3.5.11	Transmission	62
3.5.12	Film Thickness	62
3.5.13	Tensile Properties of OPEFB-NCC Film	62
3.5.14	Polarized Optical Microscope	63
3.5.15	Dispersion Stability	64
3.5.16	Contact Angle	65
3.5.17	Statistical Analysis	65
	<b>CHAPTER 4: ISOLATION AND CHARACTERIZATION OF NANOCRYSTALLINE CELLULOSE FROM OPEFB MICROCRYSTALLINE CELLULOSE</b>	<b>66</b>

4.1	Introduction	66
4.2	Experimental	67
4.2.1	Material	67
4.2.2	Isolation of OPEFB-NCC	67
4.2.3	Characterizations	67
4.3	Results and Discussion	68
4.3.1	Isolation of OPEFB-NCC	68
4.3.2	Morphological Analysis	70
4.3.3	Dispersion Stability	74
4.3.4	FTIR Analysis	75
4.3.5	Solid State <sup>13</sup> C-NMR Analysis	77
4.3.6	X-Ray Diffraction Analysis	79
4.3.7	Thermogravimetric Analysis	82
4.4	Conclusion	85
<b>CHAPTER 5: ISOLATION AND CHARACTERIZATION OF NANOCRYSTALLINE CELLULOSE FROM OPEFB PULP</b>		86
5.1	Introduction	87
5.2	Experimental	87
5.2.1	Effect of Bleaching Sequence on TO-OPEFB pulp	87
5.2.1.1	Materials	87
5.2.1.2	Production of TO-OPEFB Pulps	87
5.2.1.3	Characterizations	88
5.2.2	Comparison of TO-NCC Derived from OPEFB-Pulp and OPEFB-MCC	89

5.2.2.1	Materials	89
5.2.2.2	Isolation of OPEFB-NCC	89
5.2.2.3	Characterizations	90
5.3	Results and Discussion	90
5.3.1	Effect of Bleaching Sequence on TO-OPEFB pulp	93
5.3.1.1	Yield	93
5.3.1.2	Morphology	94
5.3.1.3	FTIR Analysis	97
5.3.1.4	Solid State <sup>13</sup> C-NMR Analysis	99
5.3.1.5	Carboxyl Content	101
5.3.1.6	Water Retention Value	103
5.3.1.7	Crystallinity	105
5.3.1.8	Thermogravimetric analysis	107
5.3.1.9	Summary	109
5.3.2	Comparison of TO-NCC Derived from OPEFB-Pulp and OPEFB-MCC	111
5.3.2.1	Isolation of OPEFB-NCC	111
5.3.2.2	Carboxyl Content	112
5.3.2.3	Morphology	113
5.3.2.4	Crystallinity	118
5.3.2.5	Thermal Stability	121
5.4	Conclusion	123
<b>CHAPTER 6: FABRICATION AND CHARACTERIZATION OF OPEFB-NCC FILM</b>		126
6.1	Introduction	126



6.2	Experimental	128
6.2.1	Material	128
6.2.2	OPEFB-NCC Film Fabrication	128
6.2.3	Characterizations	128
6.3	Results and Discussion	129
6.3.1	Chiral Nematic Property of OPEFB-NCC Suspension	129
6.3.2	Iridescent Properties of OPEFB-NCC Film	134
6.3.2.1	Effect of Film Thickness	137
6.3.2.2	Effect of Axial Ratio	140
6.3.2.3	Polygonal Structure of OPEFB-NCC Film	140
6.3.3	Effect of Plasticizer on the Properties of OPEFB-NCC Film	141
6.3.3.1	Tensile Properties	141
6.3.3.2	Transparency	144
6.3.3.3	Wettability	146
6.3.3.4	Evidence of Interaction	150
6.3.3.5	Crystallinity	153
6.3.3.6	Thermal Stability	149
6.3.4	Effect of OPEFB-NCC Axial Ratio of OPEFB-NCC Film	157
6.3.4.1	Axial Ratio of OPEFB-NCC	157
6.3.4.2	Morphology of OPEFB-NCC Film	161
6.3.4.3	Transparency of OPEFB-NCC Film	163
6.3.4.4	Iridescent of OPEFB-NCC Film	166
6.3.5	Chiral Nematic OPEFB-NCC as Template	168
6.4	Conclusion	171

<b>CHAPTER 7: CONCLUSION AND RECOMMENDATION</b>	174
7.1 Conclusion	174
7.2 Recommendation	178
<b>REFERENCES</b>	180
<b>APPENDICES</b>	195
APPENDIX A ANOVA Analysis Isolation of OPEFB-NCC from OPEFB-MCC	195
APPENDIX B ANOVA Analysis Effect of TEMPO Oxidation on OPEFB Pulp Properties	199
APPENDIX C ANOVA Analysis OPEFB-NCC Morphology	201
APPENDIX D ANOVA Analysis Effect of OPEFB-NCC Concentration on Film Thickness	202
APPENDIX E ANOVA Analysis OPEFB-NCC Film Tensile Properties	204
APPENDIX F ANOVA Analysis Effect of Concentration of Glycerol on Transparency of OPEFB-NCC Film	207
APPENDIX G ANOVA Analysis Effect of Concentration of Glycerol on Wettability of OPEFB-NCC Film	210
APPENDIX H ANOVA Analysis OPEFB-NCC Axial Ratio	213

## LIST OF FIGURES

	<b>Page</b>
Fig. 2.1 Oil palm tree.	6
Fig. 2.2 Average vegetable oil yield.	6
Fig. 2.3 The distribution of oil palm plantations in Malaysia.	7
Fig. 2.4 Cellulose molecular structure.	11
Fig. 2.5 Schematic for the formation of cellulose allomorphs.	12
Fig. 2.6 Schematic representation of the unit cells of cellulose I <sub>α</sub> and I <sub>β</sub> structure.	13
Fig. 2.7 Supramolecular distinction between cellulose I and cellulose II lies in inter –and intramolecular hydrogen bonds.	13
Fig. 2.8 Schematic representation of the plant cell walls along with the main polysaccharide components.	15
Fig. 2.9 Schematic for the isolation of the crystalline structure of cellulose by acid hydrolysis.	19
Fig. 2.10 Molecular structure of TEMPO and its derivatives.	20
Fig. 2.11 Regioselective oxidation of C6 primary hydroxyls of cellulose to C6 carboxylate groups by TEMPO/NaBr/NaClO oxidation in water at pH 10 -11.	21
Fig. 2.12 Schematic model of oxidation of primary hydroxyl on cellulose microfibril surface of TEMPO/NaClO/NaBr system.	22
Fig. 2.13 Cross-sectional representation accessible area for TEMPO mediated oxidation of C6 hydroxyl group of cellulose crystal surface.	23
Fig. 2.14 Schematic diagram of cellulose degradation by ultrasonic process.	28
Fig. 2.15 Possible uses of nanocellulose in novel applications.	31
Fig. 2.16 Supramolecular helical structures of cholesteric molecules at the liquid crystal phase.	33
Fig. 2.17 Natural material with iridescent properties.	35
Fig. 2.18 Electromagnetic spectrum.	35
Fig. 2.19 Dispersion of white light.	37

Fig. 2.20	Blue Morpho butterfly.	38
Fig. 2.21	Number of NCC related publications.	39
Fig. 2.22	Estimated production of nanocellulose.	42
Fig. 3.1	Experimental outline.	47
Fig. 3.2	Schematic representation of the preparation of different axial ratio of NCC.	54
Fig. 3.3	Sub-spectrum of NMR showing peaks assign to C4 of cellulose.	59
Fig. 3.4	The birefringence property of the sample was observed by viewing the sample through cross polarized film.	64
Fig. 4.1	Schematic of total yield for OPEFB-NCC production.	69
Fig. 4.2	TEM micrographs of OPEFB-MCC, oxidized OPEFB-MCC and OPEFB-NCC.	72
Fig. 4.3	Average length and width of sample.	73
Fig. 4.4	Dispersion state after shearing of OPEFB-NCC, oxidized OPEFB-MCC and OPEFB-MCC.	75
Fig. 4.5	FTIR spectra of OPEFB-MCC, oxidized OPEFB-MCC and OPEFB-NCC.	76
Fig. 4.6	NMR spectrum of OPEFB-MCC, oxidized OPEFB-MCC and OPEFB-NCC.	79
Fig. 4.7	X-ray diffraction patterns of OPEFB-MCC, oxidized OPEFB-MCC and OPEFB-NCC, and corresponding crystal planes.	81
Fig. 4.8	Model to represent cellulose chains, showing the d-spacing along the cellulose structure.	81
Fig. 4.9	TGA and TGA derivatives of the OPEFB-MCC, oxidized OPEFB-MCC and OPEFB-NCC.	84
Fig. 5.1	Experimental outline for Subchapter 5.2.1.	88
Fig. 5.2	Experimental outline for Subchapter 5.2.2.	89
Fig. 5.3	Kappa no of OPEFB pulp.	91
Fig. 5.4	Schematic formation of hemiacetal linkage from aldehyde.	92
Fig. 5.5	High aldehyde content of TO-OPEFB pulp with post oxidation and without post oxidation after 6 months of storage in refrigerator.	92

Fig. 5.6	Effects of bleaching sequence on yield of TO-OPEFB pulp.	94
Fig. 5.7	SEM micrographs of OPEFB (U) pulp and TEM micrographs of TO-OPEFB (U) pulp without sonication, after 15 minutes and after 1 hour of sonication.	95
Fig. 5.8	TEMPO mediated oxidation and fibrillation of cellulose by TEMPO system.	96
Fig. 5.9	FTIR spectrum of OPEFB pulps and TO-OPEFB pulps.	98
Fig. 5.10	NMR spectrum of OPEFB (OZP) and TO-OPEFB (OZP) pulps.	100
Fig. 5.11	Effects of bleaching sequence on carboxyl content of TO-OPEFB pulps.	102
Fig. 5.12	Effects of bleaching sequence on water retention value of TO-OPEFB pulps.	104
Fig. 5.13	Effects of bleaching sequence on crystallinity index of TO-OPEFB pulps.	106
Fig. 5.14	Effects of bleaching sequence on <i>d</i> -spacing (200) value of TO-OPEFB pulps.	106
Fig. 5.15	Effects of bleaching sequence on TGA and DTG curves of TO-OPEFB pulps.	108
Fig. 5.16	Schematic of total yield for OPEFB-NCC production.	111
Fig. 5.17	Effects of feedstock on carboxyl content of OPEFB-NCCs.	113
Fig. 5.18	TEM images of OPEFB-MCC, OPEFB-pulp and their respective OPEFB-NCC.	114
Fig. 5.19	Dimension range of OPEFB-NCCs.	115
Fig. 5.20	Length distribution histogram of OPEFB-NCCs.	116
Fig. 5.21	Average length and width of OPEFB-NCCs.	117
Fig. 5.22	Diffraction pattern of OPEFB-MCC, OPEFB-pulp and their corresponding OPEFB-NCCs.	119
Fig. 5.23	Effects of feedstock on crystallinity of OPEFB-NCCs.	120
Fig. 5.24	Effects of feedstock on TGA and DTG of OPEFB-MCC, OPEFB-pulp and their corresponding OPEFB-NCCs.	122
Fig. 5.25	Flowchart effects of feedstock on characteristic of OPEFB-NCC.	125

Fig. 6.1	Aqueous 0.4 % (w/w) OPEFB-NCC suspension observed between white light and polarized light.	131
Fig. 6.2	POM micrographs of OPEFB-NCC gel.	132
Fig. 6.3	Evaporation process of NCC suspension to produce multilamella structure of chiral nematic NCC film.	133
Fig. 6.4	Pitch increases and decreases reversibly on sorption and desorption of water, which associated with color changes.	133
Fig. 6.5	OPEFB-NCC film view under white light, polarized light, POM and SEM.	135
Fig. 6.6	Color changes of OPEFB-NCC film view in polarized light, and view under polarized optical microscope.	136
Fig. 6.7	OPEFB-NCC film view under polarized light respective to 156 $\mu\text{m}$ , 93 $\mu\text{m}$ and 37 $\mu\text{m}$ film thickness.	138
Fig. 6.8	OPEFB-NCC film view under POM respective to 156 $\mu\text{m}$ , 93 $\mu\text{m}$ and 37 $\mu\text{m}$ film thickness.	139
Fig. 6.9	Polygonal structure of NCC film.	141
Fig. 6.10	OPEFB-NCC film without and with 60 % of glycerol.	142
Fig. 6.11	Effect of glycerol on tensile strength, elongation at break and Young's modulus of OPEFB-NCC films.	143
Fig. 6.12	Effects of glycerol on transparency of NCC film at 600 nm wavelength.	145
Fig. 6.13	Effects of glycerol on wettability of OPEFB-NCC film.	147
Fig. 6.14	Effects of glycerol on wettability of OPEFB-NCC film at 30 s.	147
Fig. 6.15	Cross section morphology by SEM of 60% of plasticized OPEFB-NCC film.	149
Fig. 6.16	FTIR spectrum of OPEFB-NCC powder, OPEFB-NCC film and plasticized (60% glycerol) NCC film.	151
Fig. 6.17	X-ray diffraction pattern of OPEFB-NCC film, plasticized (60% glycerol) OPEFB-NCC film and OPEFB-NCC powder.	154
Fig. 6.18	Effect of crystallinity on OPEFB-NCC film formation.	155
Fig. 6.19	TEM micrographs of MAR-NCC, LAR-NCC and HAR-NCC.	159
Fig. 6.20	Length distribution histogram of OPEFB-NCC.	160

Fig. 6.21	SEM surface micrograph of LAR-NCC, HAR-NCC and MAR-NCC films, and their corresponding cross section micrograph.	162
Fig. 6.22	OPEFB-NCC films of LAR-NCC, MAR-NCC and HAR-NCC.	164
Fig. 6.23	Effects of axial ratio on transparency of OPEFB-NCC film.	165
Fig. 6.24	POM micrograph of lower axial ratio, medium axial ratio and higher axial ratio of OPEFB-NCC film.	167
Fig. 6.25	TEM micrograph of OPEFB-NCC suspension doped with borax buffer and pure OPEFB-NCC suspension.	170
Fig. 6.26	SEM-EDX analysis of OPEFB-NCC film and OPEFB-NCC film doped with borax buffer.	170
Fig. 6.27	Proposed formation of nematic order cellulose from chiral nematic cellulose liquid crystal.	171

## LIST OF TABLES

		<b>Page</b>
TABLE 2.1	Wastes from Malaysia's Palm Oil Production in 2007	8
TABLE 2.2	Characteristics of TEMPO-Mediated Oxidation Reaction of Cellulose Sample	25
TABLE 2.3	Main Centers Processing Pilot or Demonstration Plants of Different Capacity	43
TABLE 3.1	List of Chemicals Used	45
TABLE 4.1	Intensity Peak of FTIR Spectra	76
TABLE 5.1	Intensity of Carbonyl Peak of TO-OPEFB Pulp	99
TABLE 5.2	Effects of Bleaching Sequence on Maximum Decomposition Temperature and Char Residue of OPEFB and TO-OPEFB Pulp	109
TABLE 5.3	Effects of Bleaching Sequence on TO-OPEFB Pulp Properties	110
TABLE 5.4	Effects of Feedstock on Char Yield and Enthalpy Value of TO-NCCs	123
TABLE 5.7	Effects of feedstock on characteristic of TO-NCCs	130
TABLE 6.1	Effects of OPEFB-NCC on Thickness of OPEFB-NCC Film	138
TABLE 6.2	Dimension and Axial Ratio of OPEFB-NCC	1158



## LIST OF ABBREVIATIONS

4-AcNH-TEMPO	4-acetamido-TEMPO
COO <sup>-</sup>	Carboxylate anion
COOH	Protonate carboxylic acid
FTIR	Fourier transform infrared spectroscopy
HAR	Higher axial ratio
LAR	Lower axial ratio
MAR	Medium axial ratio
MCC	Microcrystalline cellulose
MPOB	Malaysia Palm Oil Board
NCC	Nanocrystalline cellulose
NCC-MCC	NCC from OPEFB-MCC
NCC-Pulp	NCC from OPEFB-pulp
NMR	Nuclear magnetic resonance
O	Oxygen
OPEFB	Oil palm empty fruit bunch
OPEFB (O)	Oxygen bleached OPEFB pulp
OPEFB (OZ)	Sequence of oxygen-ozone bleached OPEFB pulp
OPEFB (OZP)	Sequence of oxygen-ozone-peroxide bleached OPEFB pulp
OPEFB (U)	Unbleached OPEFB pulp
OPEFB-NCC	Oil palm empty fruit bunch nanocrystalline cellulose
OPEFB-MCC	Oil palm empty fruit bunch microcrystalline cellulose
P	Peroxide
POM	Polarized optical microscope
RH	Relative humidity

SEM	Scanning electron microscopy
TCF	Total chlorine free
TEM	Transmission electron microscope
TEMPO	2,2,6,6,-tetramethyl-1-piperidinyloxy
TGA	Thermogravimetric analysis
TO-OPEFB pulp	TEMPO oxidized OPEFB pulp
WRV	Water retention value
XRD	X-ray diffraction
Z	Ozone

## LIST OF SYMBOLS

%	Percentage
w/w	Weight per weight
w/v	Weight per volume
°C	Degree Celsius
psi	Pound per square inch
rpm	Revolutions per minute
L	Liter
Hz	Hertz
N	Newton
g	Gram
Pa	Pascal
s	Second
ppm	Parts per million
h	Hour
k	Kilo
M	Mega
n	Nano
μ	Micro

## LIST OF PUBLICATIONS

	<b>Page</b>
APPENDIX I	216
<p>Ahmed A. Al-Dulaimi, <b>Rohaizu R.</b> and Wanrosli W. D. (2015). Molecular characterization of nanocrystalline cellulose from empty fruit bunch using sulfuric acid hydrolysis. In The 3rd International Conference on Science &amp; Engineering in Mathematics, Chemistry and Physics 2015 (ScieTech 2015). Bali Indonesia, January 3 – February 1, 2015.</p>	
APPENDIX J	217
<p><b>Rohaizu R.</b> and Wanrosli W.D. (2014). Effect of OPEFB-NCC axial ratio on optical properties of NCC film. <b>International Journal of Chemical Engineering and Applications</b>, 5(6), 468-473. <b>From</b> Proceeding International Conference on Environmental Engineering and Development (JCCEA 2<sup>nd</sup> 2014). Sydney Australia, May 27-28, 2014.</p>	
APPENDIX K	218
<p><b>Rohaizu R.</b> and Wanrosli W. D. (2013). Production of Iridescence Nanocellulose Film from Oil Palm Empty Fruit Bunch Microcrystalline Cellulose (OPEFB-MCC). In Proceeding International Conference Chemical Engineering on Science and Applications (ChESA). Banda Aceh, Indonesia, September 18-19, 2013</p>	
APPENDIX L	219
<p><b>Rohaizu R.</b> and Wanrosli W. D. (2012). Isolation of Nanocellulose Fibres from Oil Palm Microcrystalline Cellulose. In International Symposium on Resource Efficiency in Pulp and Paper Technology. Bandung Indonesia, November 20-22, 2012</p>	

# **PENGASINGAN DAN PENCIRIAN SELULOSA NANOKRISTAL TEMPO TEROKSIDA DARIPADA TANDAN BUAH KELAPA SAWIT KOSONG**

## **ABSTRAK**

Selulosa nanokristal daripada tandan buah kelapas sawit kosong (OPEFB-NCC) telah berjaya diasingkan, dengan hasil sebanyak 67% daripada OPEFB-MCC, melalui proses kimia dan mekanikal menggunakan pengoksidaan 4-acetamido-TEMPO/NaBr/NaClO dengan bantuan ultrasonik. Imej-imej TEM menunjukkan morfologi bagi OPEFB-NCC-MCC adalah kristal selulosa yang lurus dengan panjang  $122 \pm 45$  nm, dan lebar seragam  $4 \pm 2$  nm. Analisis FTIR dan  $^{13}\text{C}$ -NMR/MAS keadaan pepejal mencadangkan pengoksidaan berlaku di kumpulan hidroksil primer (C6) rantai selulosa dan OPEFB-NCC yang terhasil kebanyakannya terdiri daripada selulosa kristal jenis I. XRD dan  $^{13}\text{C}$ -NMR/MAS menunjukkan bahawa NCC mempunyai indeks kristal yang lebih rendah berbanding bahan permulaan. Analisis terma menunjukkan OPEFB-NCC terurai pada suhu rendah berbanding OPEFB-MCC, tetapi menghasilkan kadar arang yang tinggi iaitu 46% berbanding 7% bagi OPEFB-MCC. Proses penghasilan MCC menggunakan bahan kimia dan masa, melibatkan beberapa langkah tindak balas untuk penyediaannya, oleh sebab itu bahan alternatif yang lebih ringkas seperti pulpa selulosa diperlukan. Walau bagaimanapun, kerana penghasilan pulpa selulosa juga melibatkan urutan proses pelunturan, kesan bagi urutan proses pelunturan terhadap sifat-sifat pulpa TO-OPEFB juga dikaji. Berdasarkan kandungan karboksil dan nisbah kristal yang diperolehi bagi pulpa TO-OPEFB, membuktikan bahawa pulpa OPEFB tanpa pelunturan dapat memberikan kesan yang sama seperti yang diinginkan terhadap pulpa menjalani urutan pelunturan. NCC yang diasingkan dari pulpa TO-OPEFB tanpa

pelunturan (OPEFB-NCC-pulpa) juga wujud sebagai selulosa kristal yang lurus dengan lebar purata  $5 \pm 1$  nm. Secara perbandingan, OPEFB-NCC-pulpa mempunyai nisbah paksi yang lebih besar dengan panjang purata  $224 \pm 80$  nm berbanding  $122 \pm 45$  nm bagi OPEFB-NCC-MCC. Kesannya, OPEFB-NCC-pulpa mempunyai geometri nisbah paksian yang lebih besar; walau bagaimanapun keduanya adalah setanding daripada segi indeks kristal (72%) dan kestabilan terma. Filem OPEFB-NCC kelihatan pendarrona (kesan warna pelangi) pada cahaya terkutub, yang meningkat dengan ketebalan filem tetapi disertai dengan pengurangan transparensi. Pemerhatian visual bagi filem yang dibuat daripada OPEFB-NCC bernisbah paksian rendah dan medium (dengan nilai 27 dan 45) adalah lutsinar, manakala filem dengan nisbah paksian tinggi iaitu 46 kelihatan lutcahaya. Apabila dilihat dibawah POM, filem daripada nilai paksian rendah menunjukkan pantulan warna terbesar dalam kawasan biru, manakala bagi nisbah paksian medium, ia teranjak ke kawasan hijau spektrum nampak. Dengan penambahan yang berterusan nisbah paksian, kehadiran pendarrona tidak lagi dapat dilihat. Filem OPEFB-NCC-pulpa juga menunjukkan permukaan rata, lutsinar tetapi rapuh dengan kekuatan tegangan 49 MPa, modulus Young 9.26 GPa dan 0.53% pemanjangan ketika putus. Glicerol ditambahkan sebagai pemplastik, menghasilkan filem yang lebih mudah lentur, senang dibengkok, boleh dilipat dan dipotong tanpa retak berbanding dengan filem OPEFB-NCC yang tulen. Walau bagaimanapun, filem OPEFB-NCC terplastik mempunyai sifat tegangan dan kadar kristal yang rendah, tetapi kebolehbasahan yang tinggi berbanding filem OPEFB-NCC tulen. Dengan mengambil kira kesan positif dan negatif, penggunaan 30% bahan pemplastik dicadangkan bagi penghasilan filem OPEFB-NCC. Hasil daripada kajian ini membuka laluan baru dan membentuk asas dalam usaha-usaha kajian untuk meningkatkan keupayaan sisa biojisim kepada

aplikasi nanoteknologi daripada bahan terbiodegradasi dengan cara yang selamat dan mampan.

**Kata kunci:** Tandan kosong buah kelapa sawit (OPEFB); selulosa nanokristal (NCC); selulosa mikrokristal (MCC); urutan pelunturan tanpa klorin (TCF); pengoksidaan 4-acetamido-TEMPO/NaBr/NaClO dengan bantuan ultrasonik (TEMPO); ultrasonik; nematik kiral; filem selulosa nanokristal tandan kosong buah kelapa sawit (OPEFB-NCC filem); sifat pendarrona; sifat tegangan.

# ISOLATION AND CHARACTERIZATION TEMPO OXIDIZED NANOCRYSTALLINE CELLULOSE FROM OIL PALM EMPTY FRUIT BUNCH

## ABSTRACT

Oil palm empty fruit bunch nanocrystalline cellulose (OPEFB-NCC) has been successfully isolated, with yields of 67%, from OPEFB-MCC via a chemical and mechanical process using 4-acetamido-TEMPO/NaBr/NaClO oxidation and ultrasonic treatment. TEM images indicate the morphology of OPEFB-NCC as straight crystals of cellulose with lengths  $122 \pm 45$  nm, and uniform widths of  $4 \pm 2$  nm. FTIR and  $^{13}\text{C}$ -NMR/MAS solid state analysis suggests that oxidation occurred at the site of the primary (C6) hydroxyl groups on the cellulose chain and that OPEFB-NCC consists primarily of crystalline cellulose I. XRD and  $^{13}\text{C}$ -NMR/MAS indicated that OPEFB-NCC had a lower crystallinity index than the OPEFB-MCC starting material. Thermal analysis revealed that OPEFB-NCC degraded at lower temperature than OPEFB-MCC, but had a much higher char content of 46% to the 7% of OPEFB-MCC. The production of MCC is a chemical and time consuming process, involving various reaction steps during its preparation; hence an alternative of a much simpler material such as cellulose pulp is much desired. However, since its production also entails a sequence of bleaching process, the effect of such sequence on the properties of TO-OPEFB pulps were also investigated. Based on the carboxyl content and crystallinity of the obtained TO-OPEFB pulp, it is established that unbleached OPEFB pulp gave the same desired effect than bleached TCF pulps. NCC isolated from TO-OPEFB unbleached pulp (OPEFB-NCC-pulp) also exhibit straight crystals of cellulose with an average width of  $5 \pm 1$  nm. Comparatively, OPEFB-NCC-pulp has a longer crystallite length with an average length of  $224 \pm 80$



nm against  $122 \pm 45$  nm for OPEFB-NCC-MCC. Consequently, OPEFB-NCC-pulp has a greater geometrical axial ratio; nevertheless, both types of NCC are comparable in terms of crystallinity and thermal stability. Films of OPEFB-NCC exhibit iridescence (rainbow like effect) in polarized light, which increases with film thickness but at the expense of transparency. Visual observations of the film made from low and medium geometrical axial ratios of OPEFB-NCC (with values of 27 and 45) were optically transparent, whilst the film with high axial ratio of 46 appeared translucent. When viewed under POM, film of low axial ratio induces the largest reflected color in the blue region, whilst for the medium axial ratio, it shifted to green region of the visible spectrum. With further increase to the high axial ratio, the iridescent appearance could no longer be seen. The OPEFB-NCC-pulp films also showed a smooth, transparent but brittle surface with a tensile strength of about 49 MPa, Young's modulus of 9.26 GPa and an elongation at break of 0.53%. Glycerol was added as a plasticizer, resulting in a much more pliable film, easily bent, folded and can be cut without cracking compared to that of the pure OPEFB-NCC-pulp film. However, the plasticized OPEFB-NCC-pulp films have lower tensile properties and crystallinity, but higher wettability compared to pure OPEFB-NCC film. Taking into consideration of the positive and negative effects, it is suggested that a 30% addition of glycerol is recommended for OPEFB-NCC film production. The outcome of this study opens a new avenue and forms the basis in the research efforts on expanding the capabilities of biomass residue into nanotechnology application from biodegradable material in a safe and sustainable manner.

**Keywords:** Oil palm empty fruit bunch (OPEFB); nanocrystalline cellulose (NCC); microcrystalline cellulose (MCC); total free chlorine (TCF) bleaching sequence; ultrasonic assisted 4-acetamido-TEMPO/NaBr/NaClO oxidation (TEMPO); ultrasonication; chiral nematic; nanocrystalline cellulose film (NCC-film); iridescent properties; tensile properties

## **CHAPTER 1**

### **INTRODUCTION**

#### **1.1 Project Background**

As one of the biggest producers and exporters of palm oil, Malaysia produced approximately 90 million tons of oil palm biomass each year (Danish et al., 2015); including trunks, fronds, and empty fruit bunches (OPEFB), with annual production expected to increase in line with the growing worldwide demand for palm oils (Bazmi et al., 2011). These residues represent an abundant, inexpensive, and readily available source of renewable lignocellulosic biomass.

Several applications such as electricity generation, conversion into pulp and paper products (Wanrosli et al., 2006) and roughage for animal feeds (MARDI, 2008) have been proposed for the oil palm lignocellulosic residues. To increase its diversity and economic importance, new high-performance products from this lignocellulosic based materials that are safe and sustainable have to be developed.

#### **1.2 Problem Statement**

OPEFB with ca. 60% cellulose content (Wanrosli et al., 2004), has the potential to be exploited into high value products in particular in the production of nanocrystalline cellulose (NCC). NCC are the basic building blocks of cellulose and

are nanorod in the range of 100-500 nm in length and less than 10 nm in width, depending on the cellulose source (Fleming et al., 2001; Habibi et al., 2010).

NCC are considered today as a novel class of nanomaterials with many attracting properties such as nanoscale dimension, high specific strength and modulus, high surface area, unique optical properties, etc. (Peng et al., 2011) that has the potentials to be used in an array of applications. Of particular interest which forms as one of the object of this research is the production of iridescent film, which is seen as a prospect material towards developing a lightweight visual display fabrication that could replace the currently used high conventional batch processes based on plastic (petroleum based product) substrate (Shah & Brown, 2005; Nogi et al., 2009).

NCC can be isolated from a variety of cellulose sources. Of late, considerable efforts have been geared toward producing nanocellulose from non-woody sources; such as sisal fiber (Moran et al. 2008), kenaf (Jonoobi et al. 2010; Kargarzadeh et al. 2012), pea hull (Chen et al. 2009), rice straw (Jiang & Hsieh 2013), and sugarcane bagasse (Mandal & Chakrabarty 2011). Since Malaysia has an abundant supply of oil palm fibrous material generate by the palm oil industry and this biomass is readily available at minimal cost, it is economical, of great interest to develop a technique that can process this lignocellulosis biomass into a high value product of NCC.

NCC is usually obtained from the crystalline regions of cellulose fiber via sulfuric acid hydrolysis at elevated temperatures, however, this process induces a rapid decrease in the degree of polymerization through breaking down the accessible amorphous regions of the long glucose chains resulting in yield loss, with only ca. 30

% of the crystalline obtained (Habibi et al., 2010; Peng et al., 2011; Hirota et al., 2012). Hence, alternative isolation processes are sought.

NCC's have recently been prepared via 2,2,6,6-tetramethyl-1-piperidinyloxy (TEMPO)-mediated oxidation to yield of more than 90% being reported (Kitaoka et al., 1999; Saito et al., 2007; Tahiri & Vignon 2000). In an effort to increase the efficiency of the oxidation reaction, ultrasonic uses have been proposed to assist the TEMPO-mediated oxidation.

The high energy of the ultrasound expected can give advantages in the TEMPO-mediated oxidation process through fibrillation process, thus increasing availability of accessible primary hydroxyl groups for oxidation. This seems to suggest that this is a promising route to isolate NCC from OPEFB, hence, this methodology of ultrasonic assisted TEMPO-mediated oxidation is adopted in this study.

### **1.3 Objectives**

The objectives of the present study were:-

- i. To isolate and characterize OPEFB-NCC from OPEFB-MCC using the ultrasonic assisted TEMPO-mediated oxidation followed by ultrasonification of the oxidized cellulose.
- ii. To study various degrees of lignin content (effects of total chlorine free (TCF) bleaching sequence) on the properties of TEMPO-oxidized OPEFB pulp and to isolate OPEFB-NCC from the most efficient oxidized OPEFB pulp by ultrasonification.

- iii. To compare the properties of OPEFB-NCC isolated from OPEFB-MCC and most efficient OPEFB-pulp produced in (ii).
- iv. To fabricate and characterize OPEFB-NCC film from selected OPEFB-NCC obtained in (ii)
- v. To study the effects of film thickness, geometrical axial ratio and plasticizer on the properties of NCC film produced in (iv).

## CHAPTER 2

### LITERATURE RIVIEW

#### 2.1 The Oil Palm

Oil palm (*Elaeis guineensis*) (Fig. 2.1) originated from West Africa, and later brought to Southeast Asia as an agricultural crop to produce palm oil that is derived from the palm fruit at the beginning of the 20<sup>th</sup> century. Since then, rapid expansion has occurred and by the mid-20<sup>th</sup> century, the oil palm industry has become the most important agricultural sector that contributes to high export earnings to Malaysia. It is the most productive oil crop and has become an important feedstock to the food industry for edible oil production, since the amount oil produced per hectare per year is far greater than other vegetable oils like soybean, sunflower and rapeseed (Fig. 2.2) (MPOB, 2013).

In 2011, Malaysia alone had 4.908 million hectares of oil palm plantation, which covers approximately 73% of the agricultural land (Wendy et al., 2012). Fig. 2.3 shows distribution of oil palm plantation that can provide employment opportunities to the local residents.



Fig. 2.1: Oil palm tree.

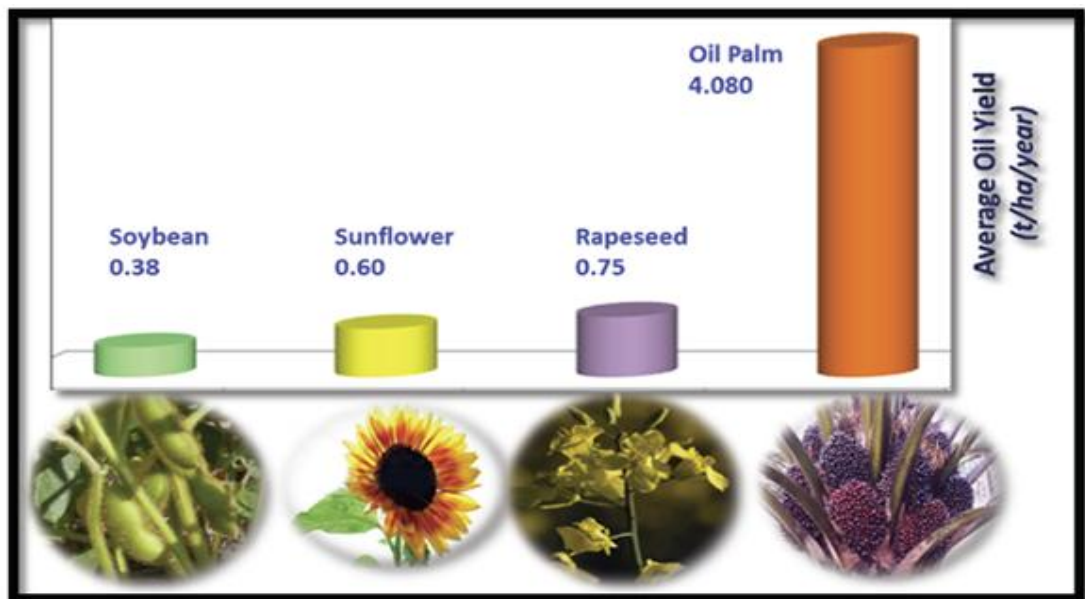


Fig. 2.2: Average vegetable oil yield (MPOB, 2013).



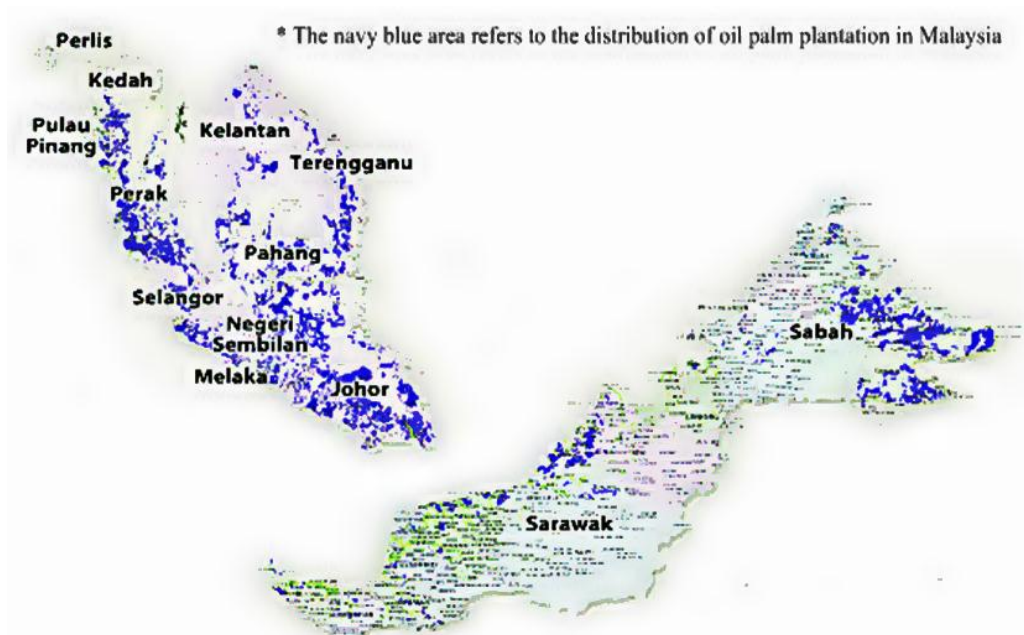


Fig. 2.3: The distribution of oil palm plantations in Malaysia (Wendy et al., 2012).

### 2.1.1 Oil Palm Biomass as an Alternative Source of Fiber

In 2005, an estimated 56 million tons of oil palm biomass are generated in Malaysia and annual production is expected to increase in line with the growing worldwide demand for palm oils (Bazmi et al., 2011). These include the oil palm fronds (OPF) and oil palm trunks (OPT) which are obtainable at the plantation site; empty fruit bunches (EFB), palm kernel shells, mesocarp fiber and palm oil mill effluent (POME) at the mill sites. TABLE 2.1 shows the breakdown of wastes from oil palm production. Although efforts are currently underway to utilize this enormous biomass, it is still perceived as wastes causing its disposal a great concern which has gained criticism from environmental groups regarding their biodiversity and air pollution (Aljuboori, 2013).

TABLE 2.1: Wastes from Malaysia's Palm Oil Production in 2007 (Abdullah & Sulaiman, 2013)

Wastes	Quantity (k tons)
Fronds	46 837
Empty fruit bunches (EFB)	18 022
Palm pressed fibbers (PPF)	11 059
Oil palm trunks (OPT)	10 827
Shell	4 506

In terms of utilization, oil palm biomass is being used in various industries. For example, EFB is being used as mulching and fertilizer in plantation or it can contribute as a solution to the renewable energy at the mill site (Bazmi et al., 2011). In addition, oil palm EFB is now viewed as a feasible alternative of coconut fiber for mattress and cushion production, which do not need to go through further cleaning process and extracting of long fiber. Other than that, EFB can also be used for medium density fiberboard production, or can be converted into paper making pulp with good printing properties and a good papermaking formation (Henghuat, 2015).

Realizing the potential of these oil palm biomasses, recently, there have been numerous ongoing efforts to increase profits from the oil palm biomass fiber by producing fuel and bio-based chemicals (Aljuboori, 2013). Additionally, oil palm biomass residue is a reliable resource because of its availability, continually production, non-hazardous, biodegradable material (Abdullah & Sulaiman, 2013) and does not compete its food production in terms of land destination (Verardi et al., 2012). Oil palm fibers are also versatile, stable and can be processed into various dimensions and grades to fit specific applications.

Several reviews and scientific papers have been published on the synthesis of cellulose and cellulose derivative from oil palm empty fruit bunch, such as cellulose

phosphate (Wanrosli et al., 2011; Wanrosli et al., 2013), microcrystalline cellulose (Haafiz et al., 2013), carboxyl methylcellulose and cellulose acetate (Djuned et al., 2014).

In general, all lignocellulosic biomass (including wood and non-wood) is composed of lignin, hemicelluloses and cellulose, with small amounts of inorganic materials. As for oil palm biomass, it is reported (Wanrosli et al., 2004) that the composition is as follows: cellulose (60%), hemicelluloses (24%) and lignin (17%); data presented is after normalization between cellulose, hemicelluloses and lignin. Although all of these components have been investigated for its use (Ren & Zhao, 2013; Sánchez, 2009), cellulose remains the most potential because of its availability and possibility of modifications.

## **2.2 Cellulose**

Cellulose, a natural polysaccharide, is the most abundant renewable biopolymer, naturally produced by plants, as well as by microorganisms. In wood, cellulose can be obtained by 42-52% and mostly located in the secondary cell wall, while more than 90% cellulose can be obtained from raw cotton, and more than 60% can be obtained from the oil palm empty fruit bunch (OPEFB) (Credou & Berthelot, 2014; Abdullah et al., 2011). Cellulose is a macromolecule, which needs to be defined on three structural levels, namely molecular, supramolecular and morphological.

### 2.2.1 Molecular Structure

Cellulose is composed from the simplest structure of a unique monomer among polysaccharides of  $\beta$ -D-glucopyranose units, linked by  $\beta$ -1,4-glycosidic bonds. The dimer cellobiose is the smallest repetitive unit of cellulose, which is formed by two glucose monomers (Fig. 2.4). In which, anhydroglucose unit is the monomer of cellulose, cellobiose is the dimer. Cellulose chain has a direction, one end being a closed ring structure and the other being an aliphatic reducing end in equilibrium with cyclic hemiacetals (Credou & Berthelot, 2014).

The number of single anhydroglucose units constituting the chain orders the chain length or degree of polymerization (DP) of cellulose. The average DP value not only depends on the origin of the raw material, but also on the potential extraction treatments like isolation, purification, and solubilization that generally cause scission of the cellulose chain (Credou & Berthelot, 2014).

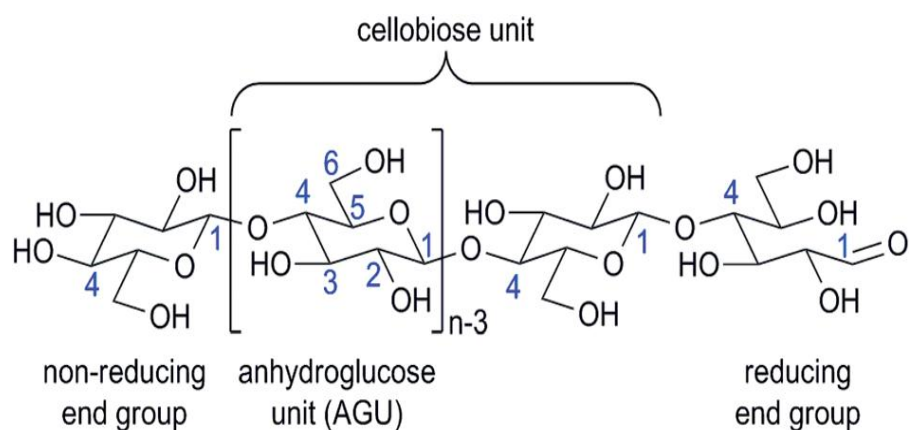


Fig. 2.4: Cellulose molecular structure ( $n$ =DP, degree of polymerization).

Cellulose contains a large amount of free hydroxyl groups available for reaction located at C2, C3, and C6 respectively, where hydroxyl group of C6 is much more reactive than that of C2 and C3 (Qin et al., 2011). These hydroxyl groups together with the oxygen atoms of both pyranose ring and the glycosidic bond have an ability to make an extensive hydrogen bond network, composed of both intra- and intermolecular hydrogen bonds that govern the physical (straightness of the chain, mechanical properties, thermal stability, etc.) properties of cellulose (Credou & Berthelot, 2014).

During cellulose formation, the intramolecular hydrogen bonds are partly responsible for linear integrity and rigidity of the polymer chain, whereas, intermolecular hydrogen bonds promote aggregation of multiple cellulose chain formation resulting in various ordered crystalline structure and other supramolecular arrangements (Credou & Berthelot, 2014).

### **2.2.2 Supramolecular Structure**

Cellulose exists in several allomorphic forms; four different polymorphs of cellulose are known as cellulose I, II, III and IV. Fig. 2.5 shows schematic for the formation of cellulose allomorphs. Indeed, two main routes from cellulose I to cellulose II, emerge by (i) mercerization (treatment with aqueous sodium hydroxide) and (ii) solubilization followed by regeneration (recrystallization). Then, treatment of cellulose I and II with liquid ammonia leads to cellulose III<sub>1</sub> and III<sub>2</sub>, respectively, and heat treatment of cellulose III<sub>1</sub> and III<sub>2</sub> leads to cellulose IV<sub>1</sub> and IV<sub>2</sub>, respectively. The transformation of cellulose III and IV is usually partial and reversible (can be converted to the origin cellulose) (Credou & Berthelot, 2014;

Kontturi et al., 2006). However, review focus on cellulose I and cellulose II due to only these cellulose allomorphs engage in this study.

Cellulose I, sometimes referred to as native cellulose, crystallizes (organize into units) simultaneously in two allomorphs of  $I_\alpha$  and  $I_\beta$  (Fig. 2.6). Cellulose  $I_\alpha$  has a triclinic unit cell and exists in primitive organism such as bacteria or algae, whereas, cellulose  $I_\beta$  has a monoclinic unit cell, and prevails in wood, ramie fibers and cotton. Fig. 2.6 (a) shows projection along the chain direction with the  $I_\alpha$  and  $I_\beta$  unit cells superimposed on the cellulose I crystal lattice, showing the parallelogram shape of both unit cells when looking down the c-axis. In this orientation both unit cells have nearly identical molecular arrangements, sharing the three major lattice planes, labeled 1, 2, and 3, with the corresponding d-spacings of 0.39, 0.53, and 0.61 (Credou & Berthelot, 2014).

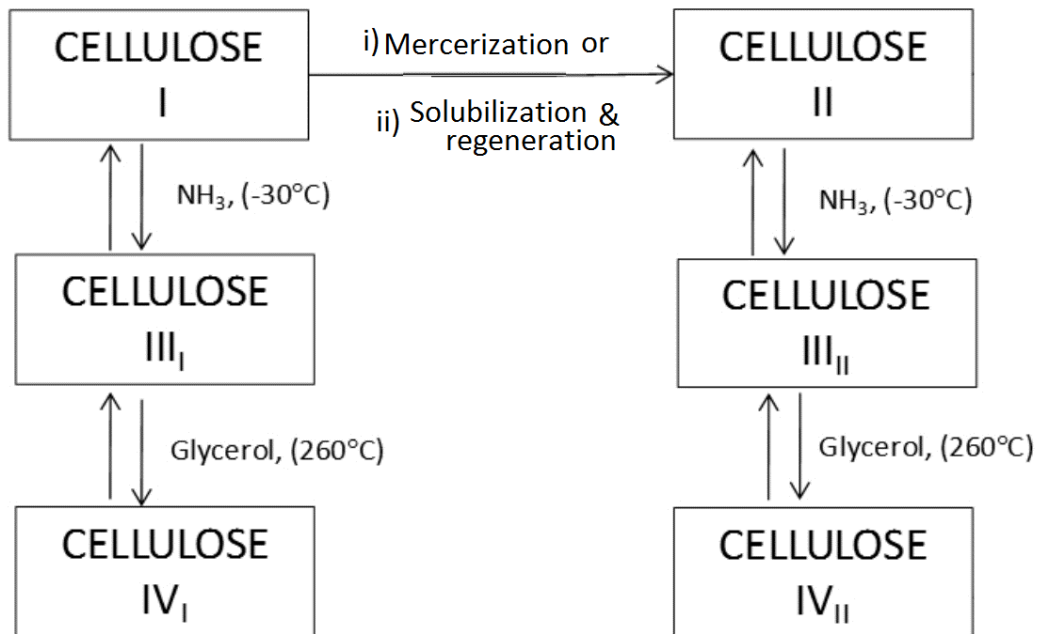


Fig. 2.5: Schematic for the formation of cellulose allomorphs.

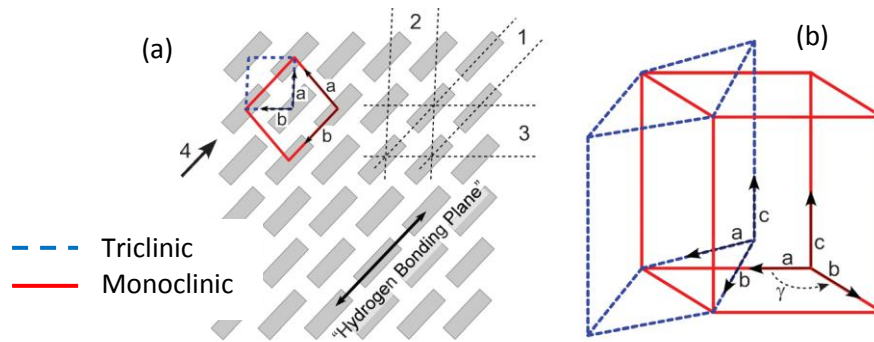


Fig. 2.6: Schematic representation of the unit cells of cellulose I<sub>α</sub> (triclinic, dashed line) and I<sub>β</sub> (monoclinic, solid line) structure (Credou & Berthelot, 2014).

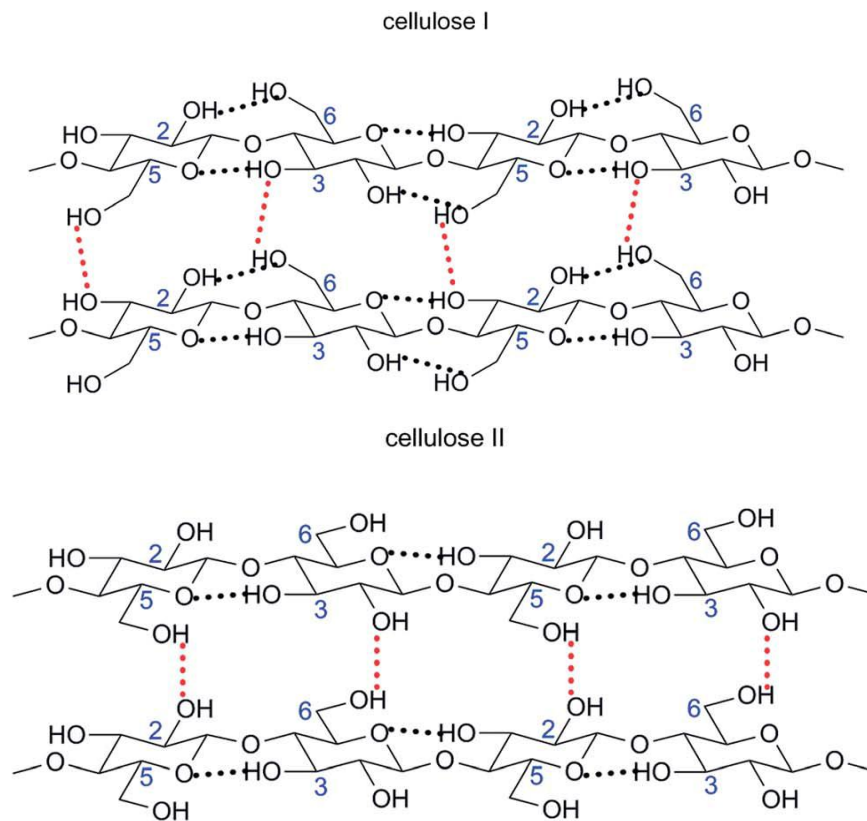


Fig. 2.7: Supramolecular distinction between cellulose I and cellulose II lies in inter- and intramolecular hydrogen bonds (Credou & Berthelot, 2014).

Cellulose I<sub>β</sub> is more stable than the I<sub>α</sub> form as the amount of weak inter-chain hydrogen bonds in the I<sub>β</sub> structures is believed to be larger than in the I<sub>α</sub> polymorph. Cellulose I<sub>α</sub> and I<sub>β</sub> are interconverted by bending during microfibril formation and

metastable cellulose  $I_{\alpha}$  converts to cellulose  $I_{\beta}$  on annealing (a process of heating and slow cooling) (Poletto et al., 2013).

Cellulose II crystallizes in the same monoclinic unit cell, but, different from their inter- and intramolecular hydrogen bonds as compared to cellulose I (Fig. 2.7). The main interchain hydrogen bond is that of O3-H $\cdots$ O5 for both polymorphs, which gives cellulose chain its rigid, linear shape. In contrast, cellulose I have an O6-H $\cdots$ O3 inter-chain bond, whereas cellulose II has it at O6-H $\cdots$ O2 position, resulting cellulose II to have an antiparallel packing whereas the chain in cellulose I run in a parallel direction.

In addition, intermolecular hydrogen bonds of cellulose II occur in the intrasheets and between intersheets to form an optimal hydrogen network bonding unlike cellulose I where only intrasheet hydrogen bonds have been detected and a slipping of sheets appears possible (Zugenmaier, 2001). Therefore, cellulose II is considered to be irreversible and thermodynamically the most stable among cellulose crystalline forms (Credou & Berthelot, 2014; Kontturi et al., 2006).

### **2.2.3 Morphological Structure**

Cellulose has a hierarchical (characteristic of a hierarchy) structure, from the polymeric glucose chains to the microfibrils (Fig. 2.8). The long chains of cellulose polymers are accumulated and packed together in a very specific way described as being fractal (complex patterns that are self-similar across different scale) to form microfibrils (nanometer scale diameter and micrometer scale length) by hydrogen and van der Waals bonds (Samir et al., 2005). Assembling these microfibrils together



results in microfibrils (micrometer scale diameter and millimeter scale length) that represent the building block of cellulose (Credou & Berthelot, 2014). This assembly leads to cellulose commonly having a highly crystalline structure, insoluble in water, and resistance to most reagents (Fleming et al., 2001; Lucia & Rojas, 2009; Montanari et al., 2005).

Cellulose can be classified as a semicrystalline fibrillar material since it contains both crystalline and amorphous regions as a result of small crystalline units being imperfectly packed together (Fleming et al., 2001; Samir et al., 2005). Their ratio, or degree of crystallinity, depends on the origin of cellulose: sisal 65-70% (Credou & Berthelot, 2014), tunicate 95% (Zhao et al., 2015), wood 40-30% (Andersson et al., 2003), cotton linter 56-78% (Terinte et al., 2011), and flax 72% (Credou & Berthelot, 2014; Cao et al., 2012a).

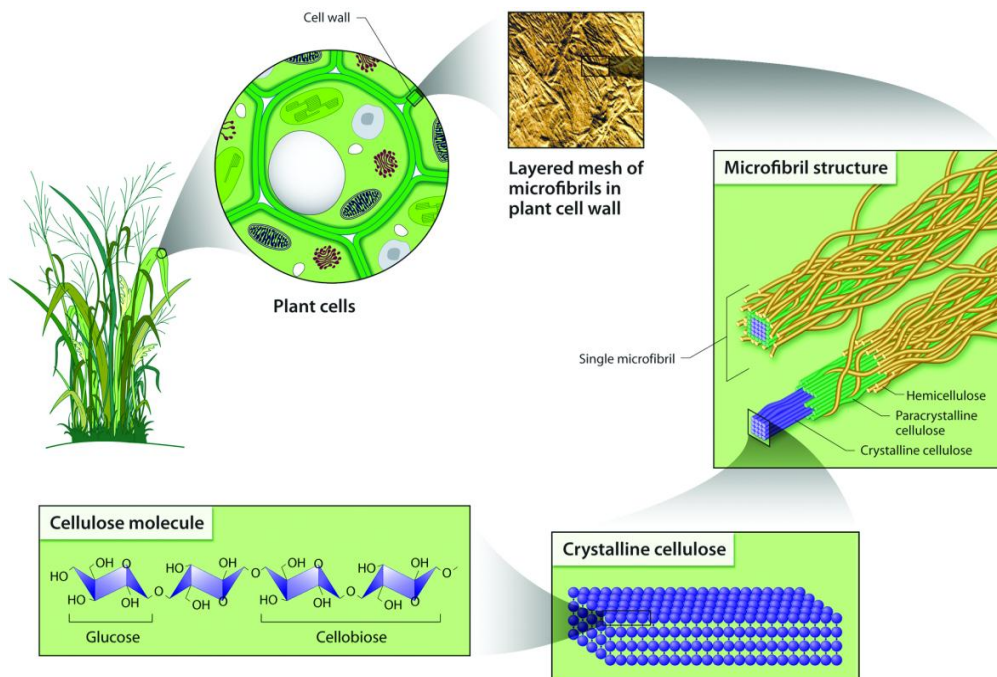


Fig. 2.8: Schematic representation of the plant cell walls along with the main polysaccharide components (Quiroz-Castañeda & Folch-Mallol, 2013).

Besides being semicrystalline, it is important to understand that cellulose rarely exists in nature in a pure single-compound entity as native cellulose always contains varying amounts of other amorphous component, including hemicelluloses (various polysaccharides) and lignin (a polyphenol) depending on refinement treatment (Kontturi et al., 2006). For instance, in the cell wall of plants, microfibrils, which are integrally embedded with hemicelluloses and lignin, are tightly hooked to one another (to form macrofibril) by multiple hydrogen bonds, that greatly responsible for the supramolecular structure of cellulose (Fig. 2.8) (Saito et al., 2007). For this reason, separation or individualization of cellulose nanofibrils from wood cellulose fibers or pulps is very difficult, needing extended of mechanical and chemical treatment.

### **2.3 Nanocrystalline Cellulose**

Nanocrystalline cellulose (NCC) is the basic building unit of cellulose that is released from the original cellulose fibers. Various terms have been used to describe NCC in the literature, including cellulose nanocrystal (Habibi et al., 2010; Qin et al., 2011), nanocellulose crystal, cellulose nanofibrils (Hamad, 2006), cellulose nanowhiskers (Chen et al., 2009), and cellulose crystallites (Fleming et al., 2001).

NCC is a one dimensional nanomaterial (1D), nanorod within the range 100 to 500 nm length with a width of less than 10 nm. However, determining the exact dimensions of NCC is complicated, where the overall size, shape and specific dimensions of the NCC depends on the cellulose origin, preparation condition (Fleming et al., 2001; Habibi et al., 2010; Qin et al., 2011; Sacui et al., 2014), and on the used measurement techniques (Mishra et al., 2011; Montanari et al., 2005).

NCC can be obtained from a variety of cellulose sources, with wood pulp being the most used (Sacui et al., 2014; Yang et al., 2013). However, since Malaysia has an abundant supply of oil palm fibrous material generated by the palm oil industry and this biomass is readily available at minimal cost, it is, economically, of great interest to develop a technique that can process this lignocellulosic biomass into a high-value product of NCC. Because it is obtained from cellulosic fibers, NCC is a renewable, recyclable and abundant form of nanomaterials, hence making it an important class of materials with vast potential applications.

#### **2.4 Production of Nanocrystalline Cellulose**

Nanocrystalline cellulose (NCC) is usually obtained from the crystalline regions of cellulose fiber via sulfuric acid hydrolysis at elevated temperatures, whereby a small amount of sulfate ester (negative charges) is introduced to the surface during the reaction, thereby giving a significant and stable colloidal suspension of NCC over sedimentation (Fleming et al., 2001; Hamad, 2006).

Fig. 2.9 shows a scheme for the isolation of the crystalline cellulose by acid hydrolysis. This process induces a rapid decrease in the degree of polymerization through breaking down the accessible amorphous regions of the long glucose chains with yields of ca. 30% of crystalline material (Habibi et al., 2010; Peng et al., 2011; Hirota et al., 2012). This is owing to lower density of amorphous region as compared to the crystalline regions of cellulose, as a result, the amorphous regions break up releasing the individual crystallites when subjected to harsh acid treatment (Peng et al., 2011).

On the other hand, if hydrochloric acid is used as a hydrolyzing agent for isolation of NCC, their dispersibility is limited and their aqueous suspensions tend to flocculate (Habibi et al., 2006), even though their characters displayed similar under TEM and x-ray diffraction patterns to the ones obtained by sulfuric acid hydrolysis (Holt et al., 2010).

Apart from acid hydrolysis treatment, NCC has also been prepared from native cellulose using TEMPO-mediated oxidation followed by mechanical disintegration of the oxidized cellulose (Johnson et al. 2009; Saito et al. 2007). TEMPO (2,2,6,6-tetramethylpiperidine-1-Oxy) and its derivative, 4-acetamido-TEMPO are water soluble catalytic oxidation systems, which have received considerable attention due to their catalytic and selective oxidation of the primary hydroxyl groups (C6) of pulp fibers. The TEMPO radical helps to introduce additional carboxylic groups on and in fibers and thus improves inter-fiber bonding strength of paper (Kitaoka, 1999; LeRoux, 2006).

Saito et al. (2007) had studied extensively the oxidation of cellulose fibers by means of TEMPO mediation. They found significant amounts of carboxylate and aldehyde groups on native cellulose while maintaining their fibrous morphology and crystallinity. This allowed them to prepare dispersions of individualized cellulose nanofibrils in water. This technique is advantageous since it does not require strong acid to hydrolyze cellulose and gives relatively high yields. Because of its added benefits, TEMPO oxidation followed by mechanical treatment will be adopted for the production of NCC from oil palm biomass.

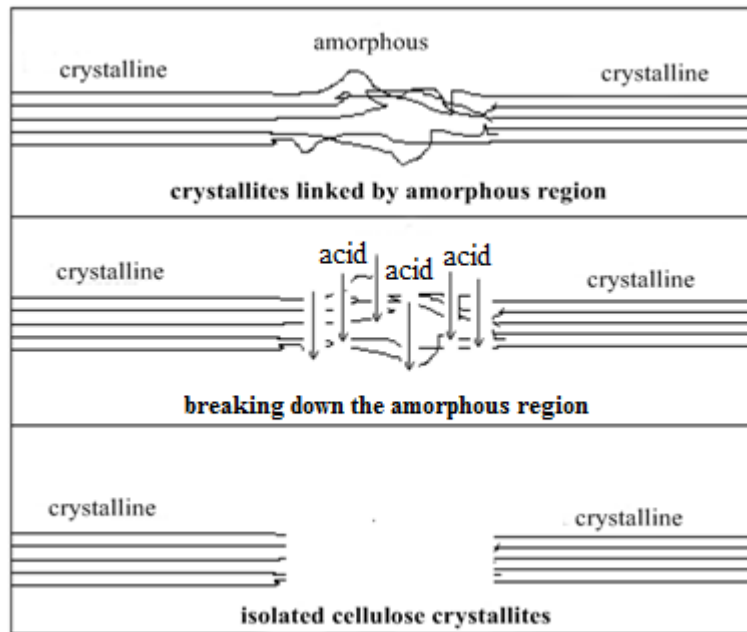


Fig. 2.9: Schematic for the isolation of the crystalline structure of cellulose by acid hydrolysis.

#### 2.4.1 TEMPO-Mediated Oxidation

TEMPO (2,2,6,6-tetramethylpiperidine-1-oxyl) and its derivatives (Fig. 2.10), are water soluble, commercially available and stable nitroxyl radicals (towards dimerization or decomposition and inert to typical organic molecules), and were studied for catalytic and high selectivity for oxidation of primary hydroxyl groups of polysaccharides under aqueous condition (Denooy et al., 1995; Qin et al., 2011; Saito & Isogai, 2004).

In general, TEMPO-mediated oxidation of polysaccharides is a regioselective process, whereby the C6 primary hydroxyl group of polysaccharides is the most prone to be oxidized to carboxylate groups than the secondary hydroxyl groups due to steric effect caused by the four methyl groups in TEMPO as well as low accessibility of the secondary hydroxyl group (Denooy et al., 1995; Saito & Isogai, 2004).

Since the dissociated carboxylate groups have anionic charges in the water, repulsive forces are formed between the cellulose microfibrils in the TEMPO oxidized celluloses with generally carboxylate contents  $>1$  mmol/g. Thus, mostly individualized cellulose nanofibrils 3-4 nm in width can be obtained by simple mechanical disintegration of the oxidized celluloses in water (Saito et al., 2006).

Initially, TEMPO-mediated oxidation was applied to water soluble polysaccharides such as pullulan, amylopectin, starch and potato. In this oxidation process, NaClO was used as primary oxidant with less than 1% of catalytic amount of NaBr (used to increase oxidation rate) and TEMPO (Denoy et al., 1994; Denoy et al., 1995; Saito & Isogai, 2004; Tavernier et al., 2008). The investigations by Saito et al. (2007) have opened new dimensions of the use of TEMPO for the isolation of NCC.

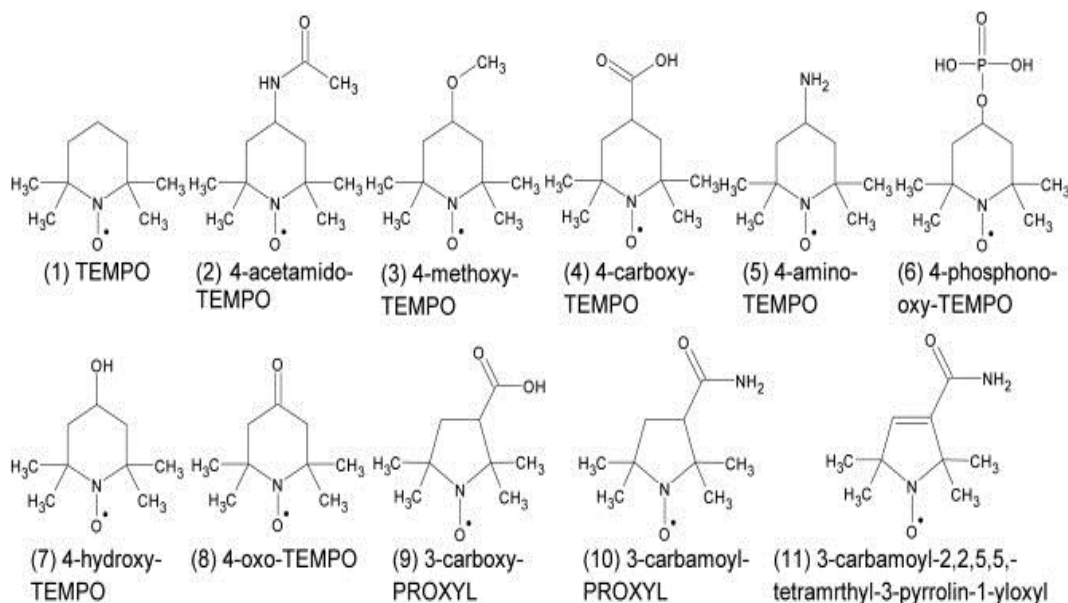


Fig. 2.10: Molecular structure of TEMPO and its derivatives (Iwamoto et al., 2010).

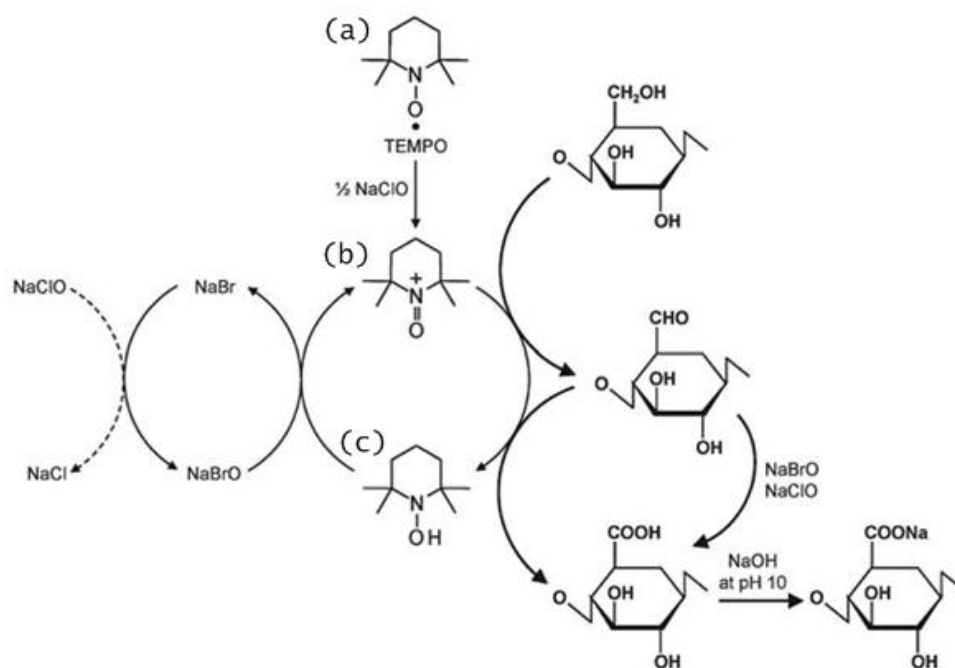


Fig. 2.11: Regiospecific oxidation of C6 primary hydroxyls of cellulose to C6 carboxylate groups by TEMPO/NaBr/NaClO oxidation in water at pH 10 -11 (Isogai et al., 2011).

The mechanism for TEMPO-mediated oxidation mechanism of cellulose is shown in Fig. 2.11. The oxidation begins with the addition of NaClO to aqueous cellulose suspensions in the presence of catalytic amounts of TEMPO and NaBr at pH 10–11 and room temperature. In this process, NaClO plays a role as primary oxidant to form NaBrO, which in turn oxidizes TEMPO (a) to form the nitrosonium compound (b). Note that the nitrosonium ion is continuously regenerated in situ. The nitrosonium compound (b) oxidizes the primary hydroxyl to carboxylate via aldehyde structure in water at pH 10, forming N-hydroxylamine (c) in Fig. 2.11. The nitrosonium compound (b) is regenerated from (c) via TEMPO in the catalytic system. The C6 primary hydroxyl groups of cellulose are converted to carboxylate groups via C6 aldehyde groups, and only inexpensive NaClO and NaOH are consumed as the oxidation proceeds (Isogai et al., 2011; Praskalo et al., 2009; Iwamoto et al., 2010).

## 2.4.2 Factors that Influence the Oxidation Reaction

Fiber morphology is one of the important factors influencing the reaction rate; TEMPO-mediated oxidation process is hampered by the high crystalline state and poor accessibility of primary hydroxyl group of cellulose materials. TEMPO-mediated oxidation of native cellulose demonstrates that even though the oxidation proceeded throughout the fibers, but only partial primary hydroxyl group could be converted mainly at the surface of the microfibrils (Montanari et al., 2005; Saito et al., 2009; Saito & Isogai, 2004; Saito et al., 2006; Tavernier et al., 2008). Therefore, most of carboxylate group were present on the crystal surface and in disorder regions with high density (Saito & Isogai, 2004). Fig. 2.12 shows a schematic model of cellulose microfibril surface oxidation by TEMPO system, in which, only primary hydroxyl group on the cellulose surface was oxidized into carboxylic group.

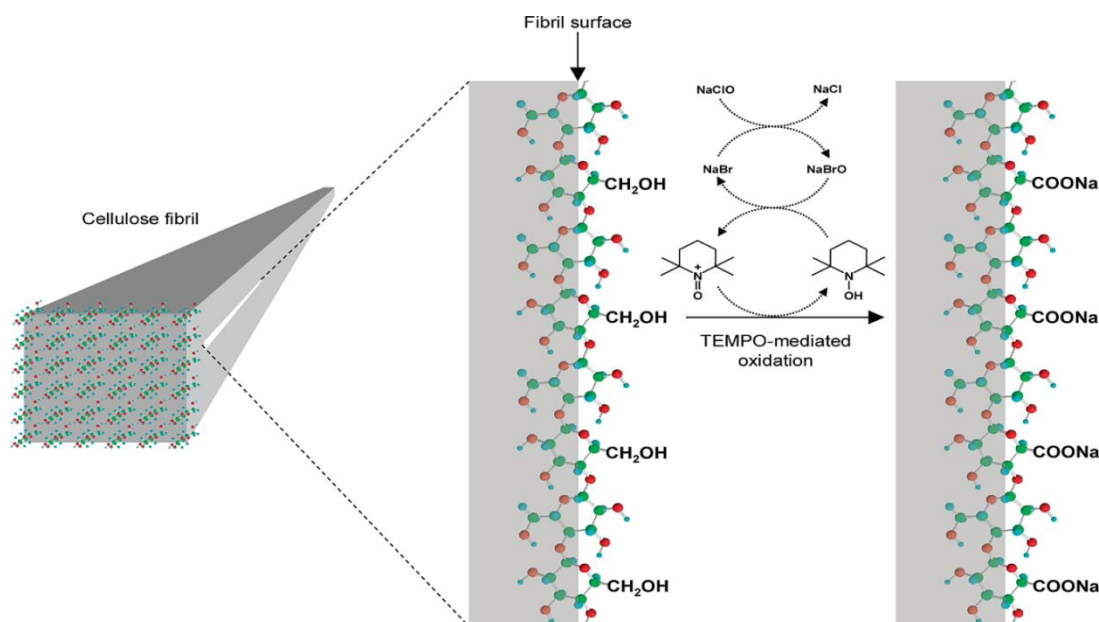


Fig. 2.12: Schematic model of oxidation of primary hydroxyl on cellulose microfibril surface of TEMPO/NaClO/NaBr system (Isogai et al., 2011).



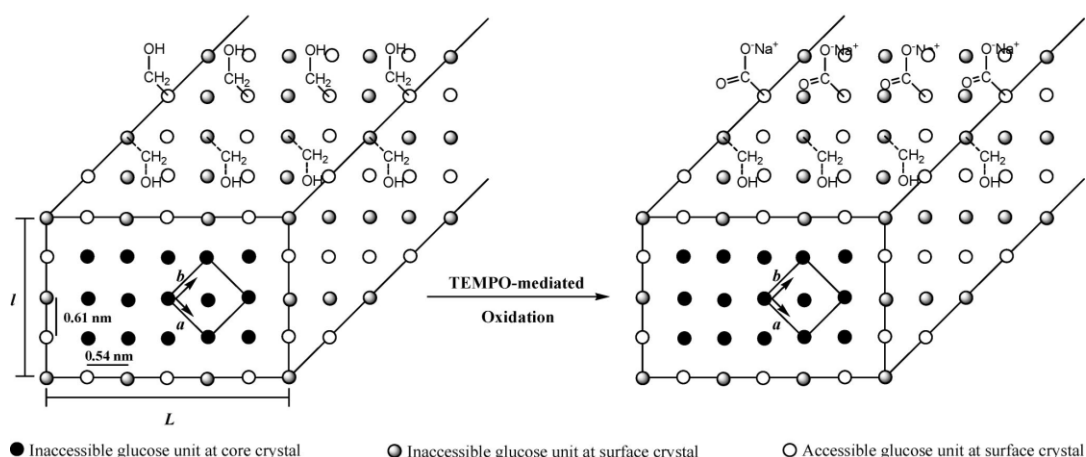


Fig. 2.13: Cross-sectional representation accessible area for TEMPO mediated oxidation of C6 hydroxyl group of cellulose crystal surface (Habibi et al., 2006).

Fig. 2.13 shows that all accessible C6 hydroxyl groups of cellulose located at the cellulose crystal surface were carboxylated, but the core of the crystals remained unaffected. The oxidation reaction can be improved either by using cellulose samples with a small microfibril diameter or, by reducing the diameter of the existing microfibrils (Habibi & Vignon, 2008; Sun et al., 2005). Therefore, ultrasonic wave was adopted in this study to reduce the diameter of microfibril during TEMPO-mediated oxidation reaction.

TEMPO-mediated oxidation is also a pH dependent reaction, which seems to be some inconsistency there with respect to the product obtained depending on the applied reaction condition, which the oxidation under basic conditions is more rapid and selective than under acid condition. Results show that the optimum pH for oxidation of water soluble glucan was between 10 – 11 (Denooy et al., 1995), while minimum depolymerization could occur in oxidation reaction of pullulan at 9.2 – 9.7 of pH range and for amorphous cellulose pH of 10 at 4°C (Dang et al., 2007). Other

than that, the molar ratio of reagent, reaction time and temperature were the key factors controlling the product yields, depolymerization of cellulose and the oxidation rate of TEMPO-mediated oxidation (Habibi & Vignon, 2008; Isogai & Kato, 1998).

As TEMPO-mediated oxidation of cellulose was studied in smaller scopes (Praskalo et al., 2009), this process may become one of the interesting and promising routes for surface modification of cellulose in the near future, where carboxylate and aldehyde functional groups can be effectively introduced into solid native cellulose under aqueous and mild conditions (Milanovic et al., 2012; Saito et al., 2006a). Furthermore, the advantages of these TEMPO-mediated oxidations are catalytic process, high reactivity rate, high yield, high selectivity, modest degradation of polysaccharides throughout the process, and consumes inexpensive hypochlorite (NaClO) and sodium hydroxide (NaOH) (Denooy et al., 1995; Praskalo et al., 2009).

TABLE 2.2 shows characteristics of TEMPO-mediated oxidation reaction of cellulose sample. Based on the review, ultrasonic-assisted treatment increases the TEMPO oxidation reaction resulting in an increase in the carboxyl content of the cellulose fibers. This is an important feature since its presence will create electrostatic repulsion between the NCC produced after mechanical disintegration of the oxidized fibers, hence maintaining their individualization for a substantial period of time. Therefore, the oxidation of OPEFB pulp in this investigation was carried out using 4-acetamido-TEMPO reaction with ultrasonic treatment at pH 9.5, which is the optimum condition for 4-acetamido-TEMPO catalyst (Mishra et al., 2012a).